Nucleic Acids Research, 2025, **53**, gkaf744
https://doi.org/10.1093/nar/gkaf744
Chemical Biology and Nucleic Acid Chemistry

Cyclic tetraadenylate binding induces dimerization of protein dimers to activate a CRISPR-associated PIN nuclease

Fang Wang [1,*,†], Pengpeng Zhao [1,†], Xiaonan Bi [1], Ruyi Zheng [1], Xuhui Tian [1], Jianan Xu [1], Suping Jiang [1,2], Guobang Li [3], Yulong Shen [1], Qunxin She [1,*]

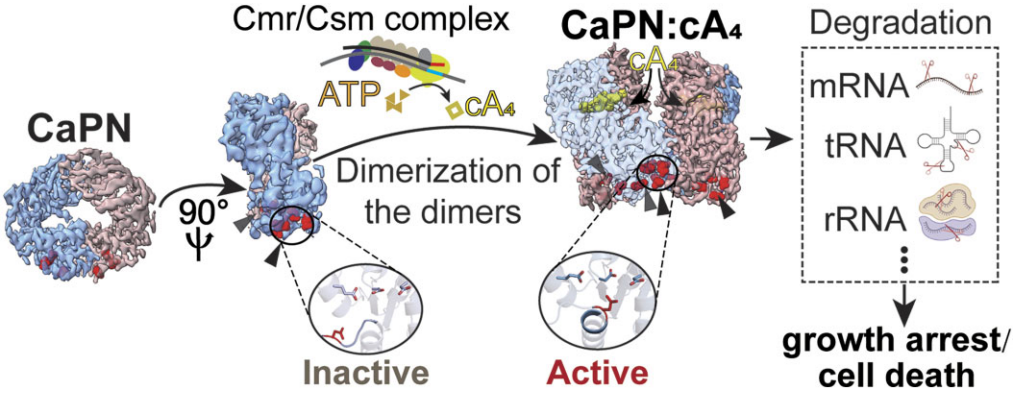
[1]CRISPR and Archaea Biology Research Center, State Key Laboratory of Microbial Technology and Microbial Technology Institute, Shandong University, Qingdao 266237, China
[2]State Key Laboratory of Agricultural Microbiology, College of Life Science and Technology, Huazhong Agricultural University, Wuhan 430070, China
[3]Institutes of Biomedical Sciences, College of Life Sciences, Inner Mongolia University, Hohhot 010021, China

*To whom correspondence should be addressed. Email: shequnxin@sdu.edu.cn
Correspondence may also be addressed to Fang Wang. Email: wangfang_sw@sdu.edu.cn
†The first two authors should be regarded as Joint First Authors.

Abstract

Type III CRISPR-Cas systems synthesize cyclic oligoadenylates (cOAs), the second messengers that bind to the CARF (CRISPR-associated Rossman fold) sensor domain and allosterically activate the effector domain of CRISPR ancillary effectors to mediate antiviral defense. An arsenal of such effectors has been identified, but only a minority of them have been characterized thus far. Here, CaPN (a CRISPR-associated PIN domain nuclease), a novel effector protein encoded by *Saccharolobus islandicus*, was characterized. Biochemical characterization of CaPN revealed that the CARF domain senses cA_4 (cyclic tetraadenylate), and its binding to the CARF domain activates the PIN domain for robust RNA cleavage. Genetic assay showed that CaPN mediates growth arrest/cell death to its archaeal host upon cA_4 sensing. Determination of the crystal structures of CaPN in apo and in the cA_4-bound form revealed that cA_4-CARF interactions trigger the conformational changes, leading to the dimerization of the CaPN dimers. These structural changes reposition D296, one of the active site residues in the catalytic pocket, to yield an active PIN domain nuclease. Together, these results unveil a novel molecular mechanism for the activation of cOA-activated Cas ancillary RNases in the CRISPR signaling pathway.

Graphical abstract



Introduction

CRISPR-Cas (clustered regularly interspaced palindromic repeats, CRISPR-associated) systems provide the adaptive immunity in archaea and bacteria to defend against invasion of mobile genetic elements such as phages, transposons, and conjugative plasmids [1–4]. Upon expression, Cas proteins form ribonucleoprotein effector complexes with mature CRISPR RNAs (crRNAs) generated from precursor crRNAs, the transcripts of CRISPR arrays, mediating antiviral defense [5]. Based on their gene synteny and interference mechanisms,

Received: April 30, 2025. **Revised:** July 2, 2025. **Editorial Decision:** July 6, 2025. **Accepted:** July 17, 2025
© The Author(s) 2025. Published by Oxford University Press.
This is an Open Access article distributed under the terms of the Creative Commons Attribution-NonCommercial License (https://creativecommons.org/licenses/by-nc/4.0/), which permits non-commercial re-use, distribution, and reproduction in any medium, provided the original work is properly cited. For commercial re-use, please contact reprints@oup.com for reprints and translation rights for reprints. All other permissions can be obtained through our RightsLink service via the Permissions link on the article page on our site—for further information please contact journals.permissions@oup.com.

Downloaded from https://academic.oup.com/nar/article/53/14/gkaf744/8222437 by guest on 14 August 2025

CRISPR-Cas systems are classified into two classes, seven types, and numerous subtypes [6, 7]. Type III CRISPR-Cas systems represent the most complex type of the immune system, which are further divided into six subtypes. To date, several subtypes III-A, -D (also named as Csm) and -B, -C (named Cmr) systems have been characterized both *in vivo* and *in vitro* [8]. These Csm/Cmr effectors are activated for the single-stranded DNA (ssDNA) cleavage that primarily targets transcriptional bubbles upon recognition of a cognate target RNA (CTR) showing mismatches between the 5′-repeat region of crRNAs and the 3′-protospace-flanking sequence of the corresponding target RNAs [9–13]. The other activated activity is the synthesis of signaling molecules, typically cyclic oligoadenylates (cOAs) [14–16], though some Cmr effectors produce S-adenosyl methionine-AMP instead [17]. cOAs function as secondary messengers that bind to Cas ancillary proteins such as Csm6 [18] and Csx1 [19], mediating antiviral defense in the CRISPR signaling pathway.

Cas ancillary proteins are also named as CARF effectors, as they have two functional domains: the CRISPR-associated Rossmann fold that binds the signaling molecule (the sensor domain) and an effector domain that mediates antiviral defense, such as the High Eukaryotic and Prokaryotic Nuclease (HEPN) domain in Csx1/Csm6, which cleaves cellular RNAs upon activation, leading to cell dormancy or cell death of infected cells. Inactivation of the signaling pathway occurs in two steps: (i) removing CTR from the type III effectors by the backbone RNA cleavage to terminate cOA synthesis, and (b) degradation of the cOA signaling molecules by RNases like ring nucleases of both host-encoded [20] and virus-encoded ones [21], as well as non-specific cOA degrader such as a membrane-associated DHH-DHHA1 family nuclease (MAD) [22].

Although structures of the sensor domains are generally conserved in these effector proteins, these CARF domains still exhibit very high diversity as they fall into 10 major clades and multiple smaller clades [23]. Yet only a few examples of CARF domains have been characterized thus far. The effector domains are even more diverse since they belong to many different types and exhibit distinct functions. Characterized effector domains include the helix-turn-helix (HTH) domain [24], transmembrane helices [25], adenosine deaminase domain [26, 27], and diverse nuclease domains such as HEPN domain [19], RelE domain [28], and the PD-D/ExK domain [29–31]. Interestingly, phylogenetic analysis revealed that the sensor and the effector domains are evolutionarily related, with distinct CARF clades typically harboring specific effector domains. For instance, the CARF3 clade frequently fused with a HTH domain [24], the CARF4 clade with the PD-D/ExK nuclease domain [29–31], the CARF5 clade with an adenosine deaminase domain [26, 27], and the CARF7 clade with the RelE toxin domain [28]. These combinations exhibit remarkable diversity both in structure features and in molecular mechanisms of antiviral defense. In this regard, the huge number of uncharacterized CARF effectors represent a large reservoir of novel antiviral defense mechanisms to be explored.

In *Saccharolobus islandicus*, SiRe_0806 encodes a protein carrying a CARFm3 domain and a PIN domain, the former is implicated in sensing a cOA signal, whereas the latter is predicted as a nuclease. However, neither domain has been characterized either alone or in a combination with other protein domain. The PIN domain, the N-terminal domain of the type IV pili twitching motility protein [32], is often not linked to cell motility and widely present in proteins of the PIN family (PFAM01850) in all domains of life [33]. In eukaryotes, PIN domains are typically an integral part of larger proteins that function in a much wider range of nucleic acid-related processes [34, 35]. In bacteria and archaea, the PIN domains are often single domain proteins such as VapCs, the toxin of the type II toxin–antitoxin (TA) system [36, 37], in which VapC toxins cleave RNA to inhibit cell growth, while their cognate antitoxins VapB block the activity of the VapC [38]. Nevertheless, all 17 *vapB* genes identified in *S. islandicus* are clustered together with *vapC* genes, forming the VapBC TA systems [39], and the *caPN* gene is not located in a proximity any of the *vapB* genes. For PIN-domain proteins, another example is the archaeal the PIN domain-P-loop NTPase (PINA) protein that remodels and processes replication forks and Holliday junctions [40]. Since the archaeal PINA protein does not show any nuclease activity, it is an intriguing question as to whether and how SiRe_0806 functions an CARF effector in the CRISPR signaling pathway.

Here we demonstrate SiRe_0806 senses cA_4, a major CRISPR signal produced by type III-B Cmr systems, and the cA_4 binding activates the PIN domain nuclease to degrade cellular RNAs to mediate growth arrest or cell death (hereafter cell death), thus representing the first known CRISPR-ancillary PIN domain nuclease (CaPN). Crystal structure analyses of the apo and the cA_4-bond forms of CaPN revealed that the PIN domain nuclease by protein tetramerization, thus uncovering a novel mechanism for the allosteric regulation of nucleases.

Materials and methods

Strains and growth conditions

Saccharolobus islandicus and *Escherichia coli* strains and plasmids used in this work are listed in Supplementary Table S1. *Saccharolobus islandicus* strains were grown at 78°C in the sucrose, casamino acids and vitamin (SCV) medium or induced for protein expression in the arabinose, casamino acids and vitamin (ACV) medium. Uracil was supplemented to 20 μg/ml if required. *Escherichia coli* strains were cultured in the Luria-Bertani medium at 37°C with shaking at 200 rpm. If required, ampicillin (Amp) was added to a final concentration of 100 μg/ml.

Construction of plasmids

Construction of expression plasmids of CaPN and its mutant derivatives

The coding sequence of the *caPN* gene (GenBank ID: 12417706) was amplified from the *S. islandicus* genome using Phanta Max Super Fidelity DNA Polymerase (Vazyme) with the primer pair of *caPN*-F/*caPN*-R, and the resulting DNA was Gibson-assembled together with the NdeI/SalI-digested *S. islandicus*–*E. coli* shuttle vector pSeSD [41] using the MultiF Seamless Assembly Mix (ABclonal), yielding pSeSD-araS-*caPN*. The plasmid was then used as the template for conducting polymerase chain reaction (PCR) to generate truncation variants (M1–M4) of araS-*caPN* using four primer pairs (caPN-Mx-F/R, where x denotes mutant numbers). In addition, the plasmid conducting site-directed mutagenesis including seven CARF residues/motifs (S9A, ^{9}SDK^{11}AAA, T14A, D38A, ^{90}RK^{91}AA, Y108A, and Y118A) and four PIN residues (D220A, D253A, D296A, and D320A) via SOE-PCR using

Downloaded from https://academic.oup.com/nar/article/53/14/gkaf744/8222437 by guest on 14 August 2025

11 primer pairs (*caPN*aaXA-F/R, where aa represents wild-type (WT) residues, X indicates mutation sites, and A denotes alanine substitution). These truncated and mutated fragments were subsequently Gibson-assembled into the NdeI/SalI sites of pSeSD, yielding expression plasmids for expressing corresponding truncation variants or CARF/PIN mutants of CaPN in *S. islandicus*.

Construction of plasmids for interference assay

For testing the CRISPR signaling based on plasmid-borne expression of CTR, pCTR-S45-araS-*caPN* was generated by amplifying the araS-*caPN* fragment from the pSeSD-araS-*caPN* template using primer pair Seq-F/Seq-R-sphIRH, followed by Gibson assembly with PaeI-digested pCTR-S45 (originally pS45GAI) [42]. For pCTR-S45-*caPN* (CARF and PIN mutants), overlap extension PCR was performed using primers ori*caPN*-F/R and *caPN*-aaXA-F/R to amplify mutagenic fragments from the *S. islandicus* genome. These fragments carrying domain-specific mutations mentioned above and 210 bp upstream sequence, including the original promoter, were Gibson-assembled into the PaeI-linearized pCTR-S45 to generate the mutant interference plasmids.

For testing the CRISPR signaling based on plasmid-borne expression of crRNA, pACSS6 was constructed using inverse PCR amplification of the pSe-RP [43] template with primers SS6-spacerF/R generated a linearized backbone, which was circularized through Gibson assembly. Finally, the original promoter-driven *caPN* fragment amplified with ori*caPN*-F/R and Gibson-assembled into PaeI-digested pSeSD and pACSS6, yielding pSe-*caPN* and pACSS6-*caPN*, respectively.

Construction of genome-editing plasmids

A CRISPR-based genome editing approach [44] was adopted to replace the original promoter of the Cmr-α system with the araS^{24M} promoter. A target sequence was identified in the promoter of the Cmr-α gene cassette with which two oligoes with the complementary sequences (Supplementary Table S2) were purchased to generate the spacer fragment. A repair template was generated with a DNA fragment containing the *cmr-4α* gene but the original promoter of the Cmr-α gene cassette was replaced with an arabinose-inducible promoter (araS^{24M}) [45]. Both DNA fragments were then inserted into a repeat-carrying vector [46], yielding pGE-araS^{24M}*Cmr-α* for mutant construction.

Plasmids transformation

All plasmids were transformed into the *S. islandicus* E233 strain or other derivative strains by electroporation, following a previously described method [47]. Briefly, ca. 600 ng of each plasmid was added into 50 μl of the archaeal competent cells and incubated for 15 min. After transferring to a 1 mM cuvette, electroporation was conducted for a single pulse with the setting of 1200 V, 25 μF, and 600 Ω. Cells were then transferred to a microfuge tube containing 950 μl incubation buffer (3 g/l potassium sulfate, 0.5 g/l potassium chloride, 0.1 g/l ammonium sulfate, and 0.7 g/l glycine, pH ≈ 5.5) and incubated at 76°C for 1 h. Aliquots of the cell suspension were mixed with 5 ml of SCV with 0.4% gelrite and plated using two-layer plating. After incubation at 76°C for 5–7 days, transformation efficiency was defined as colony formation units per μg plasmid DNA.

Expression and purification of CaPN and mutants from *S. islandicus*

CaPN and all its mutants with C-terminal 6 × His tag were expressed and purified from strain E233S containing plasmids pSeSD-araS-*caPN*, pSeSD-araS-*caPN* CARF mutants, or pSeSD-araS-*caPN* PIN mutants. The strains were cultivated on SCV plates at 78°C for ∼7 days. Subsequently, the confirmed correct transformants were streaked onto SCV plates and further cultivated for ∼3 days. The grown bacterial lawn was then transferred to SCV liquid medium for expanded cultivation. For protein expression, the strains were cultured in SCV medium for 36 h at 78°C and supplemented arabinose to the medium to induce protein expression for additional 24 h. The cells were harvested by centrifugation and resuspended in lysis buffer (50 mM Tris, 150 mM NaCl, pH 8.0), and then lysed by sonication. The lysate was clarified by centrifugation, and the supernatant was loaded onto a HisTrap HP column. The protein was finally eluted with the buffer containing 50 mM Tris, 150 mM NaCl, 500 mM imidazole, pH 8.0. Subsequently, protein purification was further performed by size-exclusion chromatography using a Superdex 200 (HiLoad 16/600) column (GE Healthcare) in buffer containing 10 mM HEPES, 150 mM NaCl, pH 7.5. The purified protein was concentrated into ∼10 mg/ml, then freshly frozen with liquid nitrogen, and stored at −80 °C for later use.

Microscale thermophoresis binding assay

The binding affinities of CaPN with cA_3 (CAS: 54447-85-7), cA_4 (CAS: 118004-81-2), or cA_6 (CAS: 232933–63-0), which were purchased from BIOLOG Life Science Institute, were evaluated by the MST binding assay using the instrument of Monolith NT.115 (NanoTemper Technologies). CaPN and its mutants were fluorescently labeled with the RED-tris-NTA dye (MO-L018, NanoTemper Technologies) in phosphate buffered saline pH 7.4 supplemented with 0.05% tween-20 (PBST). Then, 50 nM of the labeled CaPN was incubated with gradient-diluted cA_4 (from 20 to ∼0.6 nM) at room temperature for 10 min in PBST buffer. The samples were loaded into the NanoTemper capillaries (MO-K022, NanoTemper Technologies) and the binding affinity was measured at 25°C using 60% LED power and medium MST power. Dissociation constant K_d was calculated using MO. Affinity Analysis software (×86) and data fitting was performed using GraphPad Prism 9 software.

High performance liquid chromatography assay

To determine whether CaPN has the ring nuclease activities, the cA_4 cleavage assay was evaluated by an high-performance liquid chromatography (HPLC), which tracks the cA_4 and degradation products by measuring the absorbance at 260 nm. In cleavage reaction mix, cA_4 (50 μM) was incubated with CaPN (5 μM) at 70°C for 60 min in buffer containing 20 mM Tris–HCl pH 8.0 and 5 mM $MgCl_2$. Subsequently, the samples were centrifuged at 12 000 rpm for 10 min, and the supernatants were analyzed on a Prominence LC-20AT HPLC system (Shimadzu) using a hydrosphere C18 column (YMC 4.6 × 250 mm, particle size 5 μm). Samples were analyzed by gradient elution with buffer A (50 mM TEAA, pH 7.0) and buffer B (80% acetonitrile, 10 mM TEAA) as a flow rate of 0.7 ml/min as follows: 0–35 min, 0–25% B; 35–40 min, 100% B at 40°C. Degradation profiles of cA_4 were acquired by comparison with the standard cA_4 curve.

Downloaded from https://academic.oup.com/nar/article/53/14/gkaf744/8222437 by guest on 14 August 2025

In vitro DNA/RNA cleavage assay

FAM-labeled double-stranded DNA (dsDNA), ssDNA, dsRNA, and various lengths of ssRNA were synthesized by Tsingke Biotechnology Co., Ltd. (Supplementary Table S2). *In vitro* DNA/RNAcleavage assays, the FAM-labeled substrate (100 nM), CaPN protein (500 nM or gradient concentration), and cA_4 (1.5 times the concentration of CaPN) were mixed in a reaction buffer (20 mM MES at pH 6.0 and 5 mM $MgCl_2$) and incubated at 70°C for 30 min. Subsequently, the samples were subjected to electrophoresis using a 16% TBE-urea polyacrylamide gel and visualized using Amersham ImageQuant™ 800 (Cytiva). For the *in vitro* ribosome RNA cleavage assay, ribosomes of *S. islandicus* were prepared following a previously described protocol [48]. An equimolar mixture of 30S and 50S ribosomal subunits (final concentration A_{260} = 4 μg/μl), CaPN protein (3 μM or absence), and cA4 (10 μM or absence) were combined in reaction buffer (20 mM MES, pH 6.0, 5 mM $MgCl_2$). The reaction mixture was subsequently incubated at 70°C for 60 min, and the RNA products were extracted using TRIzol reagent, subsequently subjected to electrophoretic separation on a 1% (w/v) agarose gel. Total RNA of *S. islandicus* was extracted using TRIzol reagent and a 1 μg amount was used for the cleavage reaction. The reaction products were loaded onto a 0.8% (w/v) agarose gel for electrophoresis. The agarose gel was stained with ethidium bromide (EB) and cleavage products were analyzed using the gel imaging systems of Shanghai Jiapeng Technology.

In vitro tRNA cleavage assays

Transcription of various types of transfer RNA (tRNA) from *S. islandicus* was conducted *in vitro*. Initially, the T7 promoter sequence (TAATACGACTCACTATAGGG) was appended upstream of each tRNA gene sequence. Considering the relatively short lengths of these sequences (ranging from 93 to 159 bp), we designed two primers that covered the entire sequence and overlapped by ∼20 bp, allowing them to serve as templates for each other during amplification (Supplementary Table S2). The amplified tRNA gene fragments containing the T7 promoter were purified using ethanol precipitation and then used as templates for *in vitro* transcription with a kit (JT101-02, TransGen Biotech) following the manufacturer's instructions. As the last three nucleotides "GGG" of the T7 promoter are transcribed, all tRNAs synthesized *in vitro* consequently acquire a 5′-terminal "GGG" extension, which does not influence the predicted structures of the synthesized tRNAs. These tRNAs were utilized as substrate to evaluate the cleavage capacity of CaPN. The reaction mixture, consisting of CaPN (4 μM), cA_4 (6 μM), and tRNA (1 μg), was incubated for 40 min at 70°C in a buffer containing 20 mM MES (pH 6.0) and 5 mM $MgCl_2$. Subsequently, samples were loaded on an 8% TBE-urea polyacrylamide gel to electrophorese and analyzed in gel imaging systems (Shanghai Jiapeng Technology) after stained with EB. Grayscale values were quantified using ImageJ software to calculate the remaining amount of tRNA, and the results were plotted using GraphPad Prism 9 software.

Crystallization and structure determination

Crystallization of CaPN was performed at 16°C using the sitting-drop vapor-diffusion method. The protein crystallization robot mosquito LCP (SPT Labtech) was used to perform high-throughput screening of crystallization conditions. Base on the initial screening results, the pH, precipitant, additive, and other conditions were further optimized. Finally, the crystals were obtained after 4 days in drops mixing equal volumes (1.5 μl) of protein solution (5 mg/ml) and reservoir solution (0.1 M sodium acetate trihydrate, pH 4.76; 2.0 M ammonium sulfate) in 48-well plates. Crystallization of cA_4-bound CaPN complex was performed as the apo form, except that pre-incubating with cA_4 for 10 min at 70°C. The crystals were obtained after three days in drops mixing equal volumes (1.5 μl) of cA_4:CaPN complex (5 mg/ml) and reservoir solution (0.1 M Tris, pH 8.0; 40% MPD) in 48-well plates.

The apo CaPN crystals were shortly soaked in cryoprotectant (a drop of reservoir solution supplemented with 25% glycerol), while the cA_4:CaPN complex has 40% MPD in reservoir instead, and then both of them rapidly frozen with liquid nitrogen. Diffraction data of apo CaPN and cA_4-bound CaPN were collected at the beamlines BL18U1 and BL19U1, respectively, in shanghai synchrotron radiation facility (SSRF) under cryogenic conditions at 100 K [49]. Data indexing, integration, and scaling were conducted using XDS [50] and HKL3000 software suite [51]. Crystal structure was solved by molecular replacement with the Phaser program [52] using the structure predicted by Alphafold2 as search model. The structure was manually rebuilt using Coot [53] and refined in CCP4 [52] and PHENIX [54]. Data collection and refinement statistics are shown in Table 1. The protein–protein interface was analyzed on the PISA server [55]. Molecular graphics were drawn using the program PyMOL (Schrödinger). Atomic coordinates and structure factors have been deposited in the Protein Data Bank with identification code 9JXW for the apo CaPN and 9JXX for the cA_4-bound CaPN.

Table 1. Data collection and structure refinement statistics

Parameter	*CaPN apo*	*CaPN:cA$_4$*
Data collection		
X-ray source	BL18U1, SSRF	BL19U1, SSRF
Space group	$P2_12_12_1$	P1
Unit-cell dimensions		
a, b, c (Å)	86.93, 95.63, 108.82	79.47, 81.84, 86.22
α, β, γ (°)	90.00, 90.00, 90.00,	75.47, 87.09, 61.09
Resolution (Å)	43.77 – 3.00 (3.18 – 3.00)	48.82–2.50 (2.57–2.50)
Unique reflections	18 726 (2991)	58 836 (4703)
Completeness (%)	99.8 (100.0)	92.7 (94.6)
Mean I/sigma (I)	11.4 (3.5)	11.3 (2.0)
Multiplicity	5.4 (5.5)	3.6 (3.6)
R_{merge} (%)	8.6 (34.4)	4.4(43.7)
$CC_{1/2}$ (%)	99.4 (96.1)	99.9 (89.3)
Refinement		
No. reflections	18 654	58 808
R-work	0.266 (0.352)	0.208 (0.315)
R-free	0.295 (0.443)	0.244 (0.325)
B-factors	102.49	54.47
Ramachandran Favored/allowed (%)	97.25 (2.75)	97.32 (2.68)
Disallowed (%)	0	0
R.m.s. deviations		
Bond lengths (Å)	0.002	0.002
Bond angles (°)	0.553	0.542
PDB code	9JXW	9JXX

[a]Values in parentheses are for highest-resolution shell.

Downloaded from https://academic.oup.com/nar/article/53/14/gkaf744/8222437 by guest on 14 August 2025

Survival assays

For growth curve experiments, we used an arabinose promoter (ParaS^{24M}) [45]-regulated Cmr-α strain E233(ParaS^{24M}*Cmr-α*^{HD}-Δ*caPN*Δ*Csx1*Δ*SiRe_0811*) (Supplementary Fig. S6A) containing plasmids including the empty vector pSeSD, pSe-*caPN*, pACSS6, and pACSS6-*caPN*. The pACSS6 plasmid contains a mini-CRISPR cluster targeting *LacS* (Supplementary Fig. S6B), which could activate Cmr-α^{HD} to synthesize cOA. Transformants of the above plasmids were cultured in SCV medium to $OD_{600} \approx 0.8$ and were separately transferred to ACV medium with initial $OD_{600} \approx 0.08$. Then, the growth curves were plotted by measuring OD_{600} at 6, 30, 54, 66, and 78 h, respectively. Means with standard deviations of three biological replicates are reported for each experiment. Meanwhile, to further understand the growth inhibition mechanism of CaPN, we observed the morphology of cells cultured for 30 h using the inverted phase contrast microscope.

Results

CaPN is a cA_4-responsive effector of the *Saccharolobus* III-B Cmr systems

Saccharolobus islandicus REY15A contains two active III-B CRISPR systems, Cmr-α and Cmr-β, both of which are active in mediating antiviral defense in this archaeon [16, 56]. Previous researches suggested that these archaeal immune systems rely primarily on the activity of CARF domain effectors to exert immune responses whereas the DNase activity from the HD domain only plays a minor role [57]. Interestingly, this archaeon carries several CARF-containing genes in a close proximity of the Cmr-α system, including *csx1*, the first studied CRISPR ancillary gene, SiRe_0811 as well as CaPN with unique combination of a m3 subclade CARF domain and a novel PIN domain resembling those of VapC toxins [58].

To test if the PIN domain of CaPN could be active, four truncated mutants of CaPN, M1 through M4, were designed, carrying peptides of different lengths all of which encompass the predicted PIN domain (Fig. 1A). The resulting truncated genes were cloned to pSeSD [41], yielding archaeal expression plasmids from which peptides carrying the predicted PIN domain were expressed. *Saccharolobus islandicus* Δ98 kb, a spontaneous deletion mutant lacking all three above effector genes and being insensitive to the immunity of the III-B signal transduction pathway [42] was employed as the archaeal host for the experiments.

These plasmids were introduced into the Δ98kb archaeal cells by electroporation. If the PIN domain could be an active nuclease, their plasmid-borne expression would confer growth inhibition to their archaeal host, resulting in reduced efficiency of plasmid transformation. Since the transformation efficiency with each of the above plasmids was comparable to that of pSeSD, the reference plasmid, these results indicated that the PIN domain in CaPN is probably inactive, in contrast to the natural active PIN domain present in VapCs. However, when a CTR was also expressed to activate the cOA synthesis, the transformation efficiency was greatly reduced for the plasmid expressing the WT CaPN (Fig. 1A). These results suggested that the PIN nuclease has to be allosterically activated presumably through the interaction between cOAs and the CARF domain of the effector protein.

Type III CRISPR systems generate diverse signaling molecules, including cA_3, cA_4, and cA_6, which activate either distinct or the same downstream effector proteins. To uncover the precise signaling molecules recognized by CaPN, the protein was expressed in, and purified from, the natural archaeal host. The purified protein was then examined for its binding to cA_3, cA_4, or cA_6 using microscale thermophoresis (MST). We found that CaPN exhibits high affinity toward cA_4, with a dissociation constant (K_d) value of 16.9 nM, but the CARF protein basically does not interact with either cA_3 or cA_6 (Fig. 1B), indicative of CaPN being a cA_4-responsive effector.

Some CARF domain proteins are self-limiting factors such that they not only bind to cOA but also function as a ring nuclease to degrade the signaling molecule, and this provides the auto-regulation that is very important in the CRISPR signaling pathway. Several examples are known, such as the cA_6-degrading *Enterococcus italicus* EiCsm6 [59] and the cA_4-degrading SiRe_0811, another CARF-containing protein encoded in the same organism [60]. To test if CaPN could also be a ring nuclease, the purified protein was incubated with cA_4, along with SiRe_0811 as a positive reference. We found, while cA_4 cleavage products appeared in the reaction with SiRe_0811, the signaling molecule remained intact in the presence of CaPN (Fig. 1C). Thus, CaPN is not a self-limiting cOA effector and its CARF domain solely functions as a sensory element.

CaPN exhibits endonuclease activity

Since the PIN domain of CaPN most closely resembles those present in VapC toxins of the type II TA systems, CaPN was implicated in RNA/DNA cleavage. To test that, different forms of nucleic acids were incubated together with the purified CaPN protein both in the presence or absence of cA_4. We found that, while dsDNA, ssDNA, and dsRNA remained intact, ssRNA was effectively cleaved by CaPN in the presence of cA_4 (Supplementary Fig. S1A). In fact, the extent of cleavage of 5′FAM-labeled ssRNA (46 nt) is proportional to the concentration of cA_4, reaching the maximum activity when the molar ratio of cA_4:CaPN is 2 (Fig. 2A), and the enzyme is more active on longer RNA substrate (24 nt versus 67 nt) (Supplementary Fig. S1B). The substrate preference of CaPN was investigated using five 5′ FAM-labeled AU-rich ssRNAs, differing in two stretches of 3 nucleotides, one centered at position 5, the other, at position 15 (Supplementary Fig. S1C). Cleavage assays revealed that CaPN effectively cleaves RNA substrates between AU, CG, AA, GG, UU, UC, CC, and CA dinucleotides and this endoribonuclease is basically inactive toward UG, UA, CA, GA, and GC sites (Supplementary Fig. S1C).

Since VapC toxins are often active to tRNAs, we also tested whether tRNAs could be substrate of CaPN. A number of archaeal tRNAs were then prepared using *in vitro* transcription, and 34 tRNAs substrates of high quality were employed as substrate in the cleavage reaction, including three intron-containing tRNAs (Supplementary file 2). Given that CaPN cleaves ssRNA but not dsRNA, we hypothesize that the single-stranded loop regions of tRNA serve as its primary targeting sites. Consistent with our hypothesis, we found that CaPN is most active against the intron tRNAs (which theoretically expose more single-stranded regions) but cleaved non-intron tRNAs with different efficiencies (Supplementary Fig. S1D). To investigate the basis for differential cleavage efficiency

Downloaded from https://academic.oup.com/nar/article/53/14/gkaf744/8222437 by guest on 14 August 2025

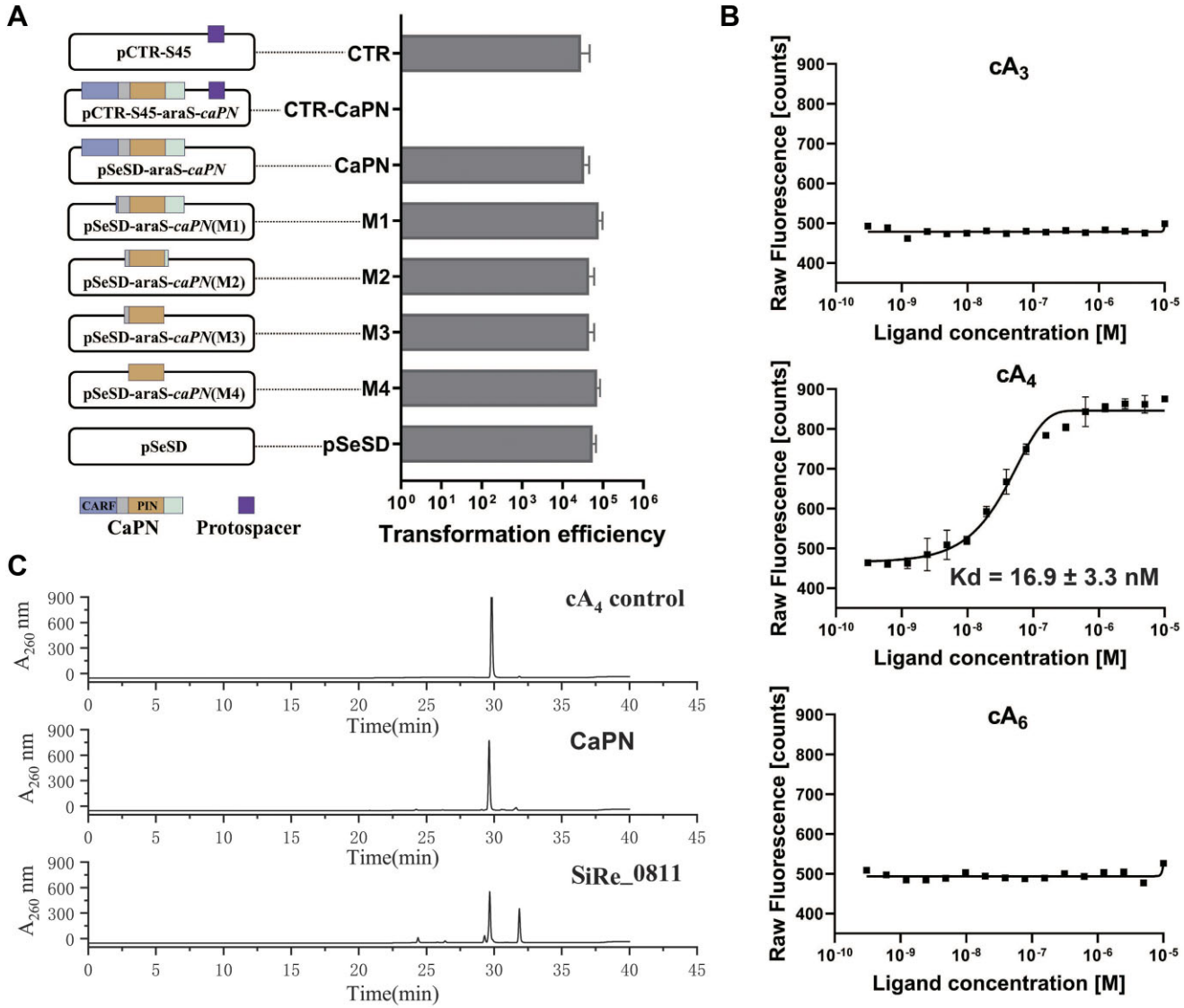


Figure 1. CaPN is a CRISPR ancillary effector to be activated by cA_4. (**A**) Transformation assay of CaPN and its truncated variants carrying the PIN domain. The assay was conducted in *S. islandicus* Δ98 kb, a strain that can produce cA_4 in the present of CTR-S45, but lacking all known CARF effector genes. CaPN and its truncated variants (M1, M2, M3, M4) are expressed as a C-terminal His-tag fusion proteins. Data are presented as mean values of three biological replicates ± SD (standard deviations). (**B**) Evaluation of the CaPN binding to cA_3, cA_6, or cA_4 using MST. Dissociation constant K_d is shown as means value ± SD, $n = 3$. (**C**) Analysis of cA_4 cleavage of CaPN by HPLC. SiRe_0811 is a known cA_4-cleaving enzyme and used as a reference.

among non-intron-containing tRNAs, we performed enrichment analysis on D-loop, anticodon-loop, V-loop, and T-loop sequences from five highly cleavable and five poorly cleavable RNA substrates. The results revealed that two types of tRNAs are relatively conserved in T-loop sequences, while highly cleavable tRNAs displayed conserved UA motifs at the 3′-terminal end of D-loop and GG motifs at the 5′-proximal region of V-loop (Fig. 2B). CaPN efficiently cleaves ssRNA substrates at the GG site but exhibits no activity toward the UA site (Supplementary Fig. S1C). Therefore, we hypothesize that GG motifs located in the 5′-proximal region of the V-loop are the preferred cleavage sites for CaPN when processing tRNA. Additionally, anticodon loops exhibited significant nucleotide divergence in two groups, with only similar nucleotide compositions enriched at the initial three position of anticodon loops (Fig. 2B). Noticeably, the organism encodes two proline tRNAs, $tRNA^{Pro}$(UGG) and $tRNA^{Pro}$(CGG), which differ by 2 nucleotides in the anticodon loop and 1 nucleotide in the V-loop, which precisely cause $tRNA^{Pro}$(CGG) forms the GG site. As expected, the enzyme exhibited robust activity against $tRNA^{Pro}$(CGG), but was barely active to $tRNA^{Pro}$(UGG) (Fig. 2B). Incubation of CaPN with the *S. islandicus* ribosome RNA and total RNAs further revealed that CaPN cleaved all types of RNAs in the presence of cA_4 molecules (Supplementary Fig. S1E and Fig. 2C). Together, these results indicated that CaPN is a robust endoribonuclease allosterically regulated by cA_4, the signaling molecule of III-B Cmr systems in *S. islandicus*.

Overall structures of the apo CaPN

The apo form of CaPN was purified from *S. islandicus*, the native archaeal host. The purified protein was analyzed by crystallization with the x-ray diffraction data and the refinement statistics are summarized in Table 1. The apo form of CaPN was crystallized in the space group $P2_12_12_1$, with two protomers in one asymmetric unit, forming symmetrical

Downloaded from https://academic.oup.com/nar/article/53/14/gkaf744/8222437 by guest on 14 August 2025

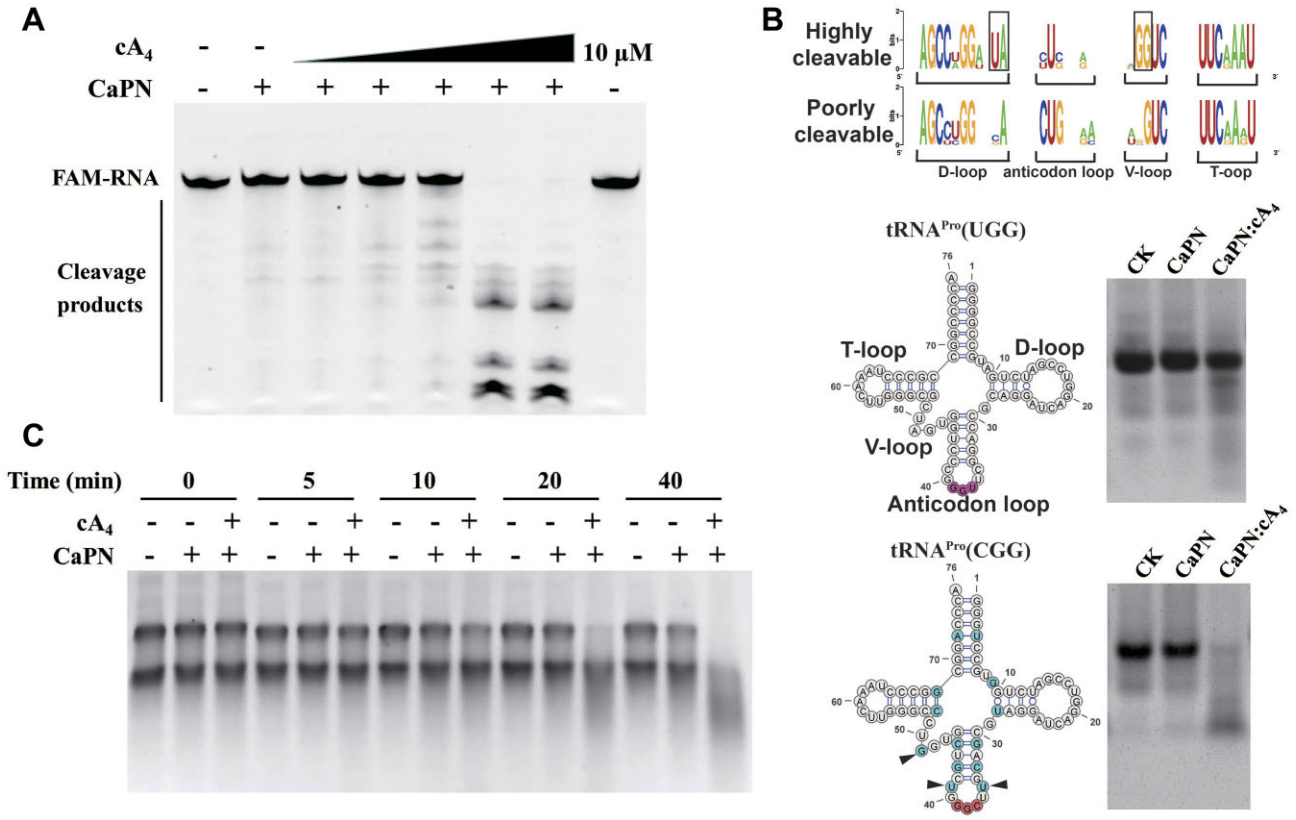


Figure 2. CaPN is cA_4-responsive endoribonuclease. (**A**) CaPN cleaves ssRNAs in a cA_4-responsive fashion. (**B**) CaPN cleavage of tRNAs shows certain sequence or structure specificity. RNA sequence enrichment analysis was conducted using the WebLogo web server (https://weblogo.berkeley.edu/logo.cgi). Structures of the two tRNAs were predicted using tRNAscan-SE 2.0 (https://trna.ucsc.edu/tRNAscan-SE/), and nucleotide bases with differences between them were highlighted with a cyan background in $tRNA^{pro}$(CGG). (**C**) CaPN is capable of shredding all types of cellular RNAs prepared from *S. islandicus*.

ring-shaped homodimer. The protein has four structural domains: an N-terminal CARF domain (residues: 1–149), a middle linker region (residues: 150–199), a PIN domain (residues: 200–344), and a C-terminal domain (residues:345–417) (Fig. 3A). Its CARF adopts a typical Rossman fold of five parallel β-sheets in the central core and four α-helices on both sides, forming an α-β-α topology. The middle linker region contains two β-sheets and two α helices, linking the CARF and PIN domains. The PIN domain also adopts Rossman fold, where β11, β12, and β13 form parallel central β-sheets that are surrounded by two sets of α-helices on the outside. The C-terminal domain possesses three β-sheets and two α helices, which, together with linker region, separates the CARF domain from the PIN (Fig. 3B). The dimerization of two CaPN protomers not only involves the two CARF but the PIN domains, and the dimerization generates a buried surface of ∼2488 $Å^2$. From a side view, the two protomers are in a misaligned fashion (Fig. 3B). Remarkably, a large central cavity is formed between the CARF and PIN domains of the protein, which is accessible to cA_4.

cA_4 binding facilitates the dimerization of the CaPN dimers

Gel filtration experiment indicated that CaPN has a molecular mass about of 80 kDa, corresponding to a dimeric form of the protein. However, addition of cA_4 to the apo form yielded a protein peak with an estimated molecular weight of 189 kDa, corresponding to a tetrameric configuration (Fig. 3C), suggesting that cA_4 binding induces dimerization of the protein dimers in solution. Indeed, the crystals of the cA_4-bound CaPN also contained four protein molecules in one asymmetric unit in which PIN domains of the two ring-shaped dimers interact with each other to form a tetramer (Fig. 3D).

The structural superposition of the two dimers within the cA_4-bound CaPN reveals a high degree of similarity (Supplementary Fig. S2A, RMSD = 0.222 Å). Therefore, we chose to describe the structural features of one of the dimers in the cA_4-bound CaPN in detail and compared with those in the apo CaPN structure. The root-mean-square-deviation (RMSD) value was 4.15 Å between the ring-shaped dimers in the two states (Supplementary Fig. S2B), indicating that the apo dimer and the cA_4-bound dimers exhibit major conformational differences. The cA_4 molecule exhibits unambiguous electron density and bound in the pocket formed by two CARF domains in the central cavity (indicated by black arrows) (Fig. 3E and F), whereas the CaPN protomers rotate relative to each other to form a more loosely dimeric conformation (buried surface is ∼1900 $Å^2$), leading to a certain degree of displacement between the two PIN domains in the side view (Fig. 3F). Superposition of individual protomer in the apo form yields a much smaller RMSD of 0.48 Å over 388 residues (Supplementary Fig. S2C), while superposition two protomers of the dimeric cA_4-bound CaPN yields a large RMSD of 1.57 Å over 392 residues (Supplementary Fig. S2D). Meanwhile, compared to the protomer A in the apo form, the

Downloaded from https://academic.oup.com/nar/article/53/14/gkaf744/8222437 by guest on 14 August 2025

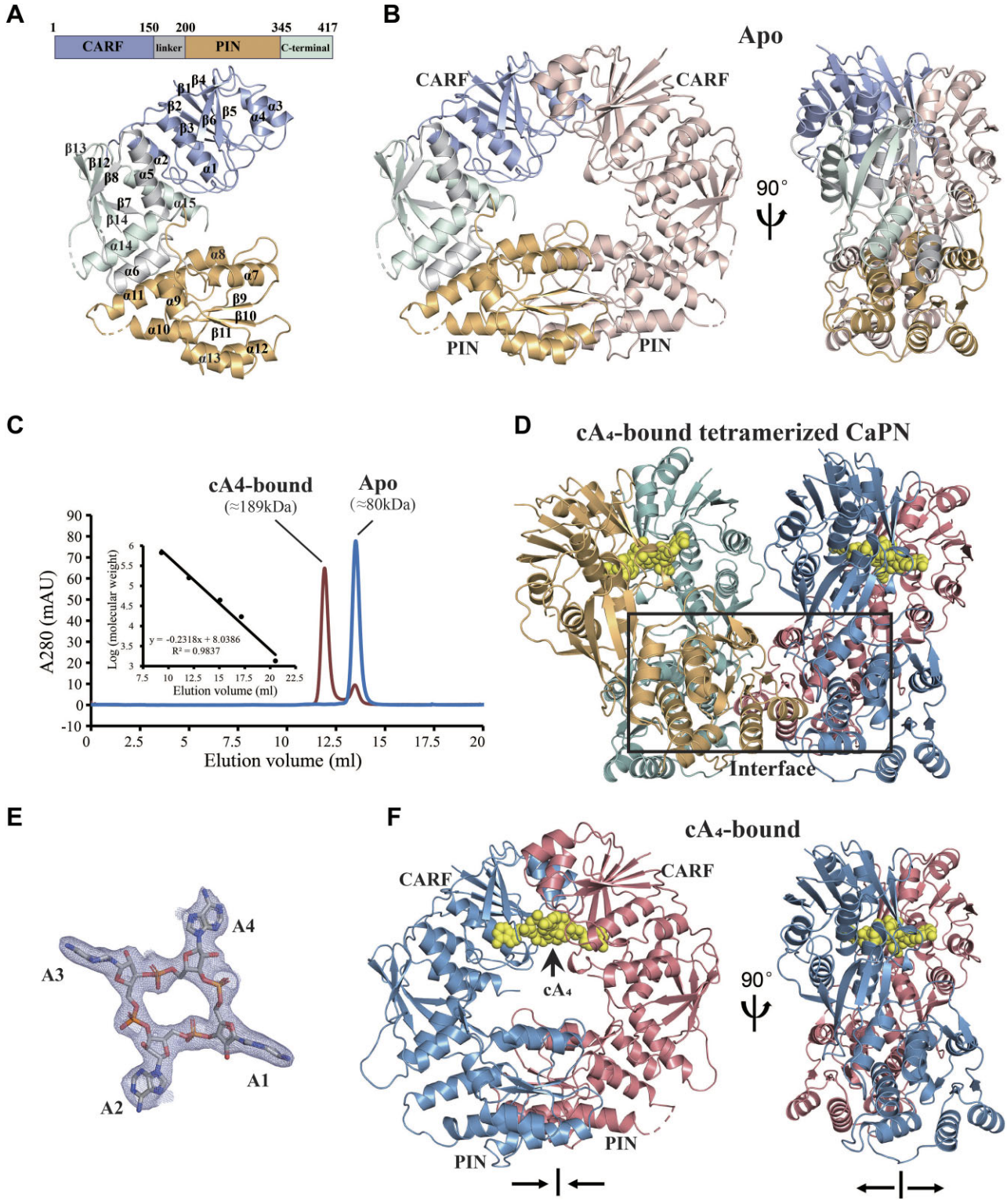


Figure 3. Crystal structures of CaPN in apo and in the cA_4-bound state. (**A**) Domain architecture and protomer structure of the CaPN protein with annotated secondary structural elements. (**B**) Main view and side view of the overall structure of CaPN in the apo form. (**C**) Detection of the oligomeric state of CaPN upon binding to cA_4 using chromatography. (**D**) The overall structure of the cA_4-bound CaPN tetramer. The four promotor chains are colored in yellowish orange (chain A), salmon (chain B), light teal (chain C), and sky blue (chain D), respectively. The cA_4 molecules are shown as yellow spheres. The interaction interface formed between the two dimers is marked with black boxes. (**E**) The 2Fo–Fc electron density map (contoured at 1.0 σ) of cA_4 in the CaPN:cA_4 complex. (**F**) Main view and side view of a half tetrameric structure of CaPN in the cA_4-bound form.

Downloaded from https://academic.oup.com/nar/article/53/14/gkaf744/8222437 by guest on 14 August 2025

B and D protomers in the cA_4-bound form exhibit significant conformational transitions (with RMSD values of 1.57 Å and 2.75 Å, respectively) (Supplementary Fig. S2E and S2F). This suggests that cA_4 binding induces two distinct conformational transitions in CaPN: [1] a relative rotational movement between the two protomers and [2] the internal conformational changes, with the extent of these changes differing between the two protomers. The structural displacement induced by cA_4 binding reshapes the interaction interface between the PIN domains. In the apo CaPN structure, dimerization engages 5 residues in the PIN domain: S246 of Chain A forms two hydrogen bonds with two residues in Chain B, i.e. D312 and E311, and vice versa; the other pair of amino acids involved in hydrogen bond formation is N309 from chain A and K248 from chain B (Supplementary Fig. S3A, left panel). Upon cA_4 binding, the interaction within PIN domain is solely maintained by hydrogen bonds formed between two residue pairs (T288 and S246, as well as N309 and R280), resulting in a diminished interaction interface compared to the apo state (Supplementary Fig. S3A, right panel).

cA_4 binding also triggers the conformational remodeling, leading to dimerization of the CaPN dimers via symmetric interactions between the PIN domains in each dimer. A multitude of residues are involved in the formation of the tetrameric CaPN, collectively defining three distinct interaction interfaces within the oligomer. The interaction interface formed by chain A and chain D is structurally equivalent with those formed by chain B and chain C, each stabilized by ∼20 residues via salt bridges and hydrogen bonding interactions (Supplementary Fig. S3B, green box). Additionally, Chain A interacts with Chain B through extensive hydrogen bonding and salt bridge interactions contributed by 14 residues (Supplementary Fig. S3B, blue box), together with chains AD and BC interfaces, maintain the formation of the tetramer.

cA_4 recognition by CARF domain of CaPN

The RNase activity of CaPN is activated upon cA_4 binding to the CARF domain. Structural comparison reveals conformational changes in three pairs of loops positioned above the cA_4 binding pocket, and these loops tend to adopt a tighter configuration after binding to cA_4 (Fig. 4A and B, top panel). Consistently, the positively charged cA_4-binding pocket formed by the CARF domain is exposed in the apo form but becomes covered in the cA_4-bound state due to the tightening of the upper region (Fig. 4B). In summary, cA_4 binding facilitates the conformational transition of the binding pocket of the CARF domain from an open to a closed form.

To reveal the detailed mechanism of ligand recognition, we defined interactions between cA_4 and CaPN. The cA_4 molecule engages in symmetrical interactions with the CARF domain of each protomer via hydrogen bonds, salt bridges, π–π stacking and π-cation interactions (Fig. 4C). In detail, the ribose-phosphate backbone and base of cA_4 forms an extensive hydrogen-bonding network with the side chain of residues ^{9}SDK^{11}, T14, D38, R90, and Y108, as well as the main chain of residues G89, K91 and Y118. Additionally, the phosphate group of cA_4 forms salt bridges with residues K11 and K91. Furthermore, the base of A1 and A3 form π–π stacking with residue Y118, while the base of A2 and A4 form π-cation interactions with residue R90. All these interactions collectively maintain the binding of cA_4 to CaPN (Fig. 4C). Among the cA_4-binding residues, the subjacent residues ^{89}GRK^{91} and Y108, exhibit minimal positional changes whereas the superjacent residues ^{9}SDK^{11}, T14, D38, and Y118 undergo significant positional shifts as loop movements (Fig. 4D). These shifts move toward the cA_4 binding pocket, enabling these residues to bind to and cover cA_4 molecule, and thereby closing the pocket.

To functionally characterize these residues, alanine substitution was conducted for key residues S9, T14, D38, Y108, and Y118 individually, and double substitution of R90 and K91 as well as a triple substitution (S9, D10, and K11), and this yielded seven mutated CaPN proteins for MST assay and RNA cleavage assay. We found: (i) D38A and Y108A mutations slightly reduced the ligand binding and RNase activity of CaPN; (ii) S9A, T14A, and Y118A substitution as well as the triple substitution (at positions of ^{9}SDK^{11}) basically abolished the ligand binding of the CARF effector, yet retaining certain levels of ssRNA cleavage in the presence of cA_4; and (iii) the double substitutions at positions ^{90}RK^{91} simultaneously abolished both the cA_4 binding ability and the RNase activity of CaPN (Fig. 4E and F). These results indicated that while S9, T14, Y118, and ^{9}SDK^{11} residues play critical roles in the binding of the cA_4 ligand, ^{90}RK^{91} residues function both in cA_4 binding and in the RNase activation.

A structural similarity search with the DALI server [61] revealed that the CARF domain of CaPN is structurally related to that of TsuCard1 (PDB: 6XL1, RMSD = 2.6 Å) [31], but they also showed important differences. TsuCard1 binds to both cA_4 and cA_6 signaling molecules, while CaPN shows binding specificity only for cA_4 (Fig. 1B). Structural superposition reveals that the CARF domain of CaPN has an extra pair of short α-helices above the cOA binding pocket compared to TsuCard1 (which has a short loop instead), and these α-helices in CaPN would clash with adenine residues A3 and A6 of cA_6 (Supplementary Fig. S4A), offering a structural explanation for CaPN's inability to bind cA_6. Superposing the cA4-bound structure of these two proteins also revealed distinct cA_4-binding features: while TsuCard1 utilizes both the CARF domain and a spatially adjacent PD-D/ExK domain loop (Loop336-341) for cA4 binding (Fig. S4B), CaPN exclusively employs its CARF domain to binds cA_4 (Fig. 3F, Supplementary Fig. S4B); nevertheless, CaPN compensates for this structural difference through the additional short α-helical pair. The Residue Y118 in this additional short α-helical pair of CaPN and L339 in the Loop336-341 of TsuCard1 occupy comparable positions relative to cA_4 and interact with cA_4 via π–π stacking and hydrophobic contacts, respectively (Supplementary Fig. S4C). In TsuCard1, this structural element is replaced by a PD-D/ExK loop (Loop336-341) where a conserved AA interact with cA_4 through hydrophobic contacts (Supplementary Fig. S4). Further comparison of cA_4-binding residues revealed semi-conserved interaction patterns. Key CaPN residues S9, K91, and Y108 are structurally conserved in TsuCard1, with D38 in CaPN replaced by E41 in TsuCard1, retaining equivalent negative charge. Beyond these similarities, CaPN and TsuCard1 exhibit distinct residue compositions and spatial arrangements for cA_4 recognition (Supplementary Fig. S4C). Overall, CaPN interacts with cA_4 via 10 residues in one protomer, and this number in TsuCard1 is 7, indicative of divergent evolution for CARFm3 (CaPN) and CARF4 (TsuCard1) in cA_4 recognition.

Downloaded from https://academic.oup.com/nar/article/53/14/gkaf744/8222437 by guest on 14 August 2025

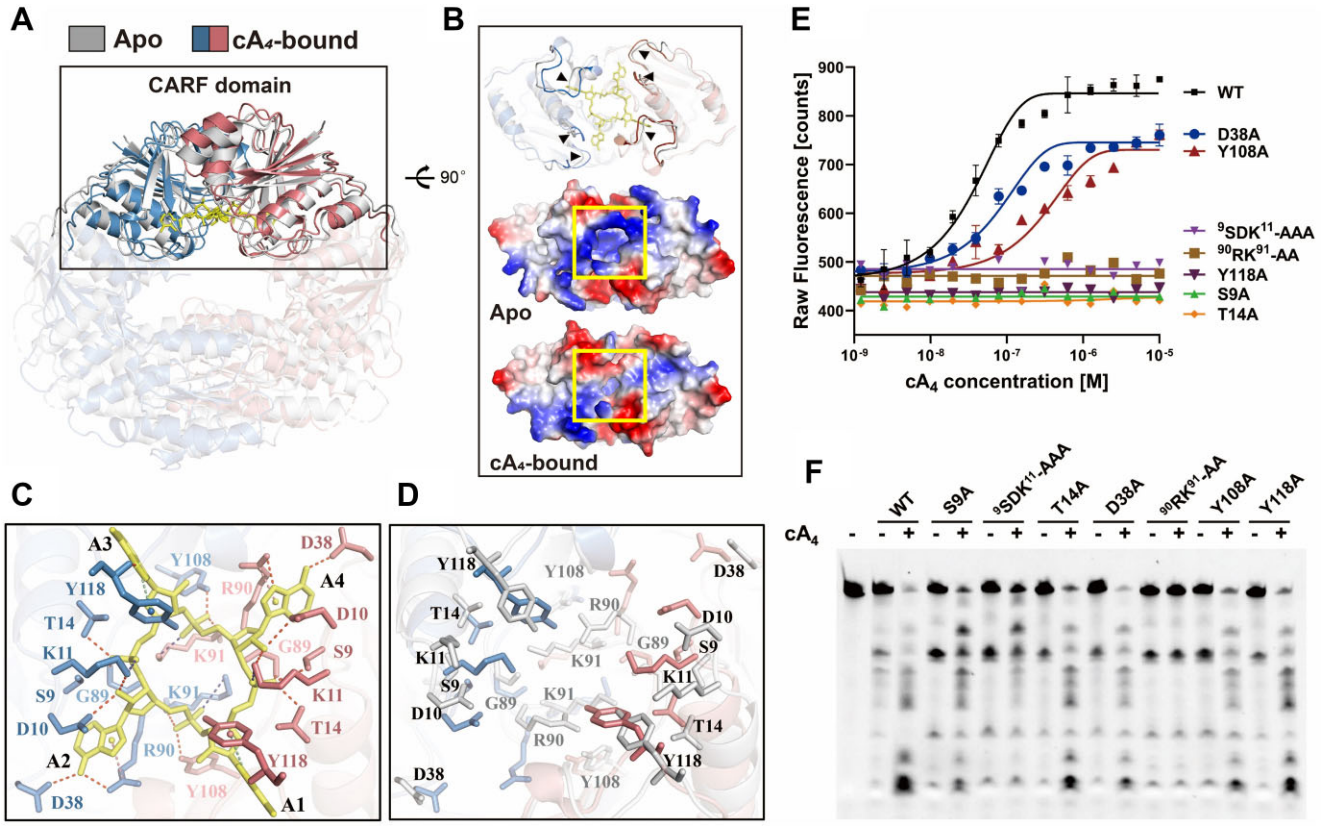


Figure 4. Structure-function relationship of the CaPN CARF domain. (**A**) Structural comparison of the CARF domain of CaPN in apo (gray) and in the tetrameric cA_4-bound state (only half of the circular tetramer is shown, and the dimeric protomers are in salmon and sky blue, respectively). The CARF domain is highlighted by setting the transparency of other domains to 80%. The cA_4 signaling molecule is displayed in yellow sticks. (**B**) Cartoon and electrostatic surface view of the CaPN CARF domain in apo and in the cA_4-bound state. Loops above the cA_4 binding pocket are marked with triangles in the cartoon illustration. (**C**) Interactions between cA_4 and the conserved binding site residues in the CARF domain. AMPs of cA_4 was shown as sticks and numbered as A1-A4. Binding site residues in the CARF domain are shown as sticks and highlighted in the same color as the protomer domain. The dotted lines represent the interactions as hydrogen bound (red) salt bridges (blue), π–π stacking (palegreen) and π-cation interactions (wheat). (**D**) Comparison of the structural positions of the ligand-binding residues in the CARF domain in cA_4-bound CaPN and in the apo form. (**E**) MST assay of cA_4-binding affinity by CaPN and its CARF domain mutants. Dissociation constant K_d are means ± SD, $n = 3$. WT CaPN, $K_d = 16.9 \pm 0.33$ nM; D38A, $K_d = 64.3 \pm 14.77$ nM; Y108A, $K_d = 262.4 \pm 66.04$ nM; Other mutants, no binding detected. (**F**) ssRNA cleavage assay of CaPN and CARF domain mutant proteins.

cA_4-dependent activation of the CaPN PIN domain

Sequence alignments of the CaPN PIN domain with homologous sequences revealed four conserved acidic amino acid residues (D220, E253, D296, D320; CaPN numbers) (Fig. 5A), which are likely the catalytic residues in the active site of the PIN domain. To reveal the mechanisms of CaPN activation, we analyzed the overall structure of the CaPN PIN domain in the context of the apo and cA_4-bound forms. The results indicate that the relative positions of the two PIN domains are shifted in the two different forms, such that two active centers in the cA_4-bound dimer are pushed away from each other relative to those in the apo form (Fig. 5B). Since the cA_4-bound CaPN is a dimer of the dimers, the four PIN domains are brought into a closer proximity (Fig. 5B and Supplementary Fig. S3B).

Careful examination of the four PIN domains indicates that they have adopted essentially the same structures, including the four conserved acidic amino acids, D220, E253, D296, and D320. Noticeably, three of the four conserved acidic residues (D220, E253, and D320) maintain the identical positions in both the cA_4-bound and apo states, whereas D296 adopts a distinct conformation: in the apo form, this residue is located away from the catalytic core; however, it refolds into the terminal segment of an α-helix upon cA_4 binding, positioning closer to the active site akin to its counterpart in VapC proteins that are naturally active (Fig. 5C and Supplementary Fig. S5) [33]. Thus, we reasoned that the apo CaPN dimer could be inactivated by mispositioning of D296 in its PIN catalytic center, whereas CaPN tetramerization positions D296 to a VapC-like conformation to activate the CARF effector. If so, all four acidic amino acids should be essential for the CaPN nuclease activity. Indeed, alanine substitution of each of these four conserved residues abolished CaPN RNase activity (Fig. 5D). Together, these results indicated that CaPN has evolved the mechanism of inactivation of the PIN domain by restructure one of the key amino acids, which can be remodeled by cA_4 binding to exert ligand-responsive regulation.

CaPN exhibits cytotoxicity upon activation by cA_4

Saccharolobus islandicus REY15A harbors two Type III-B CRISPR-Cas systems (Cmr-α and Cmr-β), with Cmr-α exhibiting robust activity of cOA synthesis [16, 56]. In Cmr-α, the Cmr2 HD domain performs non-specific DNA

Downloaded from https://academic.oup.com/nar/article/53/14/gkaf744/8222437 by guest on 14 August 2025

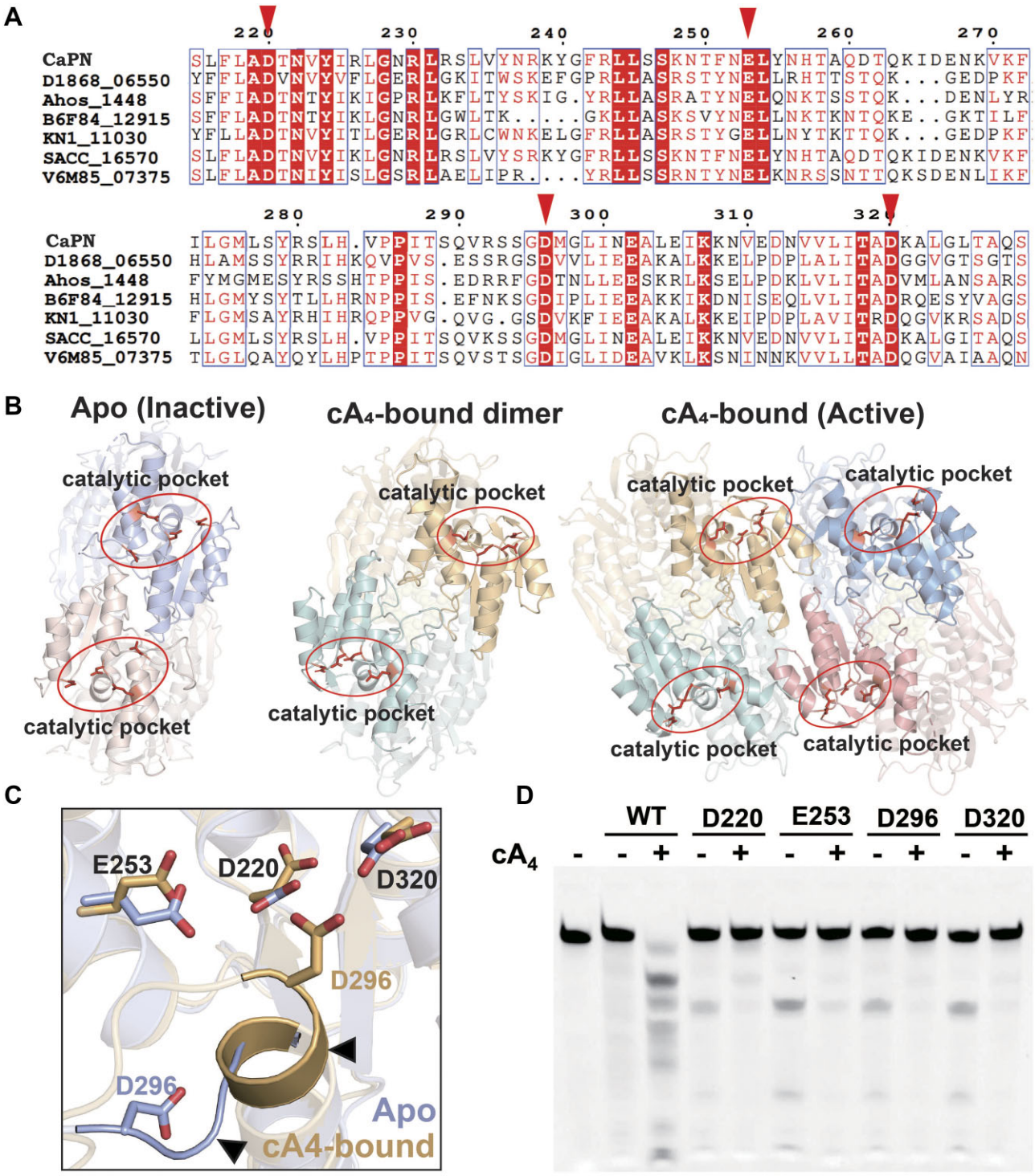


Figure 5. Structure-function relationship of the CaPN PIN domain. (**A**) Sequence alignment of the CaPN PIN domain with those from a selected set of the homologs. Conserved residues are indicated with red arrows. (**B**) Structural comparisons of the conserved residues in the catalytic pocket of the PIN domain in apo and in the cA_4-bound form. The transparency of PIN domain was set to 40%, while the other domains was set to 80% in the overall structure. The active site residues are shown as sticks and highlighted in red. (**C**) Superposition of predicted catalytic residues of the PIN domain in apo and in the cA_4-bound form. (**D**) ssRNA cleavage assay of CaPN and mutant proteins carrying substitution in the conserved catalytic residues.

Downloaded from https://academic.oup.com/nar/article/53/14/gkaf744/8222437 by guest on 14 August 2025

cleavage, whereas the Palm domain performs the cOA synthesis upon activation [16]. To construct a strain that solely relies on the CRISPR signaling for antiviral defense, we used a Cmr-α^{HD} (*ΔpyrEFΔcaPNΔCsx1ΔSiRe_0811*::Cmr-α^{HD}) strains that is deleted three known CARF-containing proteins and devoid of DNA cleavage but retains the capability of cOA synthesis. To achieve tightly control cOA synthesis, the original promoter of the Cmr-α^{HD} was replaced with the D-arabinose-inducible ParaS^{24M} promoter, yielding a cA_4-producing strain ParaS^{24M}Cmr-α^{HD}(*ΔpyrEFΔcaPNΔCsx1ΔSiRe_0811*::ParaS^{24M}Cmr-α^{HD}), that facilitates sensitive detection of CRISPR immunity from the CRISPR signaling pathway (Supplementary Fig. S6A and B).

Next, pSeSD, pSe-*caPN*, pACSS6, and pACSS6-*caPN* were introduced into the ParaS^{24M}Cmr-α^{HD} strain. The resulting transformants were then cultured in ACV to induce the synthesis of Cmr-α^{HD} for cA_4 production, and their growth was monitored by measuring OD_{600}. We found that strains carrying either pACSS6 (activating cOA synthesis) or pSe-*caPN* (expressing the CaPN protein) grew at a rate comparable to that of the strain carrying pSeSD, a reference plasmid. However, the growth of the archaeal cells carrying pACSS6-*caPN* is completely inhibited (Fig. 6A), indicating that CaPN is an effector of cOA signaling pathway and it mediates cell growth arrest in the CRISPR signaling pathway. Microscopic examination of cell samples collected 30 h after induction further revealed a marked increase in cell size for pACSS6-*caPN*-containing cells, suggesting that CaPN may inhibit cell division (Fig. 6B).

Since we did not observe any major difference in testing the function of CARF effectors in the CRISPR signaling pathway between *S. islandicus* Δ98kb and the Cmr-α^{HD}, genetic characterization of conserved amino acid residues in the CARF and PIN domains was only conducted in the Δ98kb strain. Western blot analysis revealed that there were no significant changes in the expression levels of WT CaPN or mutant CaPN with mutations in the CARF or PIN residues when CTR-S45 was absent (Supplementary Fig. S6C). Subsequently, the transformation efficiency assay was employed conducted to simultaneously express CTR-S45 along with CaPN or its mutants (Fig. 6C). We found that the R90K91 motif is crucially important for cA_4 interaction since their alanine substitutions completely abolished the CRISPR immunity, whereas alanine substitution of any other conserved residue/motif only impaired the immunity (Fig. 6D **CARF**). By contrast, substitution of any of the four PIN active site residues completely abolished the CRISPR immunity (Fig. 6D **PIN**). These results indicated that both CARF and PIN domains are required for mediating the CRISPR immunity in the Cmr signaling pathway in *S. islandicus*, reinforcing the conclusion obtained from the biochemical characterization of this novel type of CARF effector.

Discussion

Effector proteins of cOA signaling pathways possess a CARF domain to sense the cOA signaling molecule and an effector domain to execute antiviral defense. The ribonuclease effector domains characterized thus far include HEPN and RelE domains showing RNase activity, Can2/Card exhibiting both ssDNA and RNA cleavage activities [28, 31, 59]. Here, we resolved the structure of the PIN domain-containing effector CaPN and compared that with the structures of other known RNase effectors (Supplementary Fig. S7). Strikingly, the ligand-bound CaPN is a tetramer composed of two symmetrical rings, representing the first example of CARF nuclease effectors activated by the cA4-induced protein tetramerization.

The CARF domain of CaPN is most closely related to that of Card1/Can2 among the characterized CARF proteins. Indeed, their CARF domains are located in a cavity of their structures, and thereby exposed inwards, and this is in contrast to the CARF domains of Csx1/Csm6, Cami1, and Csx1-Crn1 that are exposed outwards (Supplementary Fig. S7). Interestingly, Csx1/Csm6 [59, 62, 63], Cami1 [28], and Csx1-Crn1 [64] show cA_4 cleavage activity, whereas Card1/Can2 [30, 31, 65] and CaPN do not. These findings suggest coevolution of inward CARF domains with the loss of the ability to cleave cOA ligands.

Upon binding to cOA, the CARF domain of effector proteins typically activates their function by inducing varying degrees of conformational changes in the effector domain. In some instances, such as with Cami1, cA_4 binding causes the entire effector domain to shift, with the RelE dimer moving diagonally by ∼15Å relative to the CARF-wHTH, enabling RelE domain to fit into the ribosome cleft to cleave mRNA [28]. In other cases, such as with Cad1, binding to cA_4 results in only very minor structural changes, with only the specific catalytic histidine (H448) shifting by 2Å toward the metal ion in the deaminase pocket, contributing to the formation of a catalytically competent site for the conversion of ATP to ITP [26].

To date, CaPN represents the only known CARF effector that is a dimer in the apo form, and it is activated by dimerization of the dimers. The cA_4-induced tetramerization not only alters the overall positioning of the four active sites but also remodels the position of the active residue D296 (Supplementary Fig. S3B and Fig. 5C). Notably, the D296 residues in protomers A and B mediate inter-dimer interactions via hydrogen bonds with T262 from the opposing dimer (Supplementary Fig. S3B). This interaction reorients the side chains of D296 in protomers A/B to point closer to their respective active centers relative to protomers C/D (Supplementary Fig. S5B), suggesting that protomers A/B are the primary catalytic subunits. Protomers C/D may still contribute to RNA cleavage, as their D296 main chains are also positioned on the α-helix proximal to the active site and could become catalytically competent through side-chain rotations upon substrate engagement. Activation via oligomerization has been documented for SAVED effectors like Cap4, triggered by the recognition of specific cyclic oligonucleotide signals such as 3′,2′-cGAMP and 3′,2′-cAAA by its SAVED domain, leads to conformational rearrangement of the N-terminal DUF4297 endonuclease domain and activates the promiscuous DNA cleavage to restrict phage replication [66]. Nevertheless, CaPN represents the first example of the CARF effectors to be activated via oligomerization. Multiple sequence alignments of the members of the CARF m3 clade [23] including CaPN revealed that they differ substantially in sequence identity (26%–84%) in the structural domain of cA_4 binding. Furthermore, even lower sequence identities are found for the amino acid residues involved in tetramer formation in CaPN s (5%–37%), except for D296, which is also part of the active site in the PIN domain. Therefore, whether or not the oligomerization mechanisms of CaPN's homologs could be conserved in the CaPN homologs remains to be experimentally demonstrated. However, the conservation of the

Downloaded from https://academic.oup.com/nar/article/53/14/gkaf744/8222437 by guest on 14 August 2025

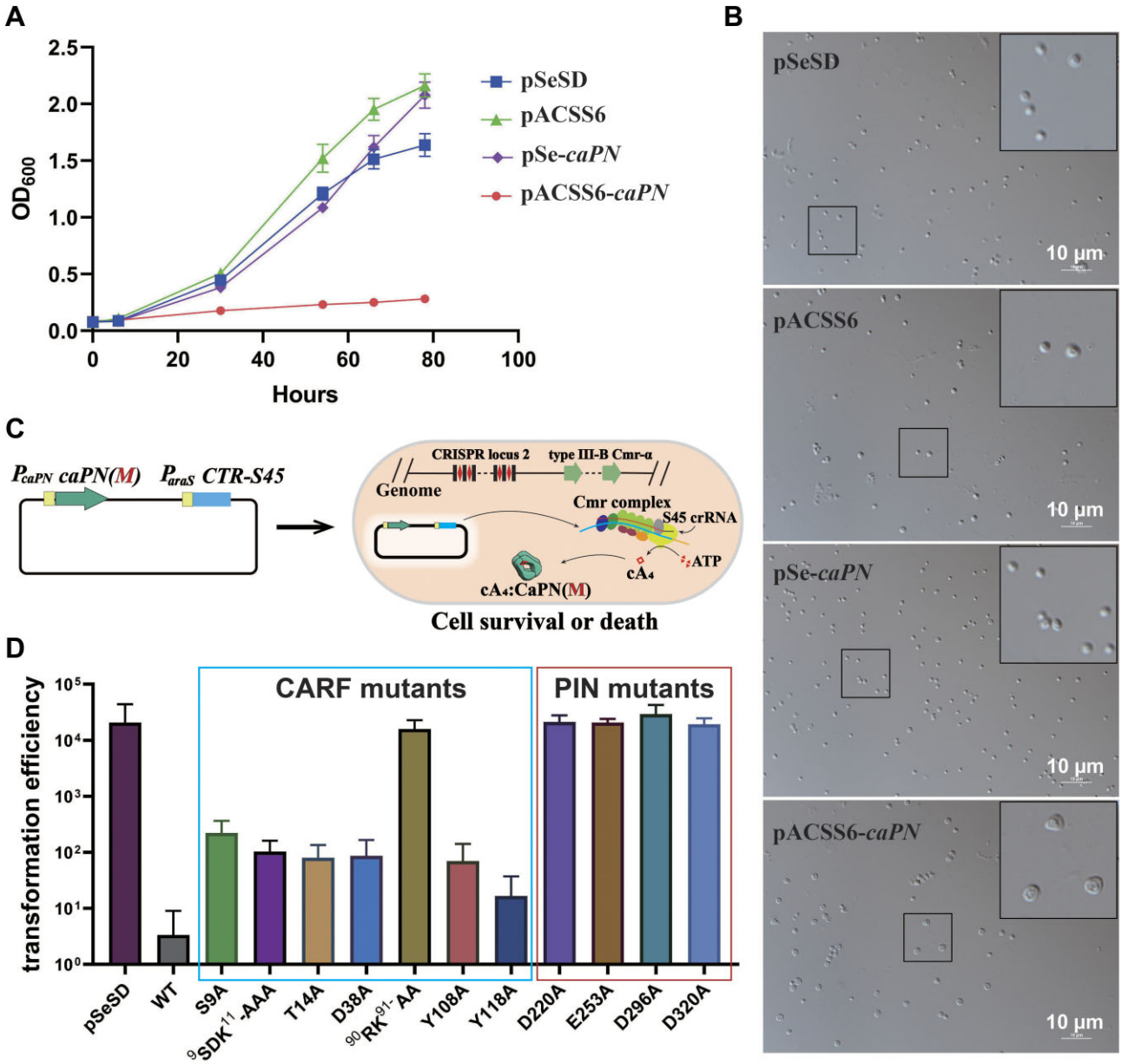


Figure 6. Functional characterization of the CaPN CARF and PIN domains (**A**) Activation of CaPN by CRISPR signaling strongly inhibits the growth of the archaeal host. pSeSD: reference plasmid; pACSS6: producing SS6 crRNAs that are complementary with a sequence of *lacS* mRNA (CTR), thereby activating the cOA synthesis from the host encoded III-B Cmr systems; pSe-*caPN*: plasmid expressing CaPN from its original promoter; pACSS6-*caPN*: plasmid producing both SS6 crRNAs and CaPN. Data are presented as the mean of three biological replicates ± SD. (**B**) Inverted phase contrast microscopy of *S. islandicus* cells. Archaeal cells of each treatment were cultured for 30 h from which cell samples were taken and analyzed. (**C**) A schematic diagram of transformation assay of CaPN and its mutants. The recombinant plasmids were electroporated into the Δ98 kb strain to generate the protospacer CTR-S45, targeted by the 45th spacer in CRISPR locus 2, and to express the effector protein CaPN or its mutants utilizing their original promoter, leading to cell death when the effector is active or cell survival when it is inactive. (**D**) The transformation efficiencies of various *caPN* plasmids, which express either WT CaPN or mutant CaPN with mutations in the CARF or PIN residues, were assessed as the schematic diagram. Data are presented as the mean of three biological replicates ± SD.

PIN active residues (95%–100% identity) among these CaPN homologs suggest that they probably exhibit very similar nuclease activity (Supplementary Fig. S8). Together, our research pinpoints that diverse modes of oligomerization provide an important means for the allosteric regulation of the activity by cOA effectors.

To prevent any excessive responses from the activated effector proteins, many effector proteins have evolved a self-inactivation mechanism to degrade cOA in the same CARF domains (e.g. Csm6 [59]). In addition, microbial hosts and viruses also encoded ring nucleases to specifically target cOAs for degradation, reducing cellular concentration of the signaling molecules. Since CaPN does not exhibit cA_4 degradation activity, the cA_4-responsive responses have to be terminated by other signal-degrading enzymes. Indeed, *S. islandicus* encode ring nucleases SiRe_0455 [67] and SiRe_0811 [60] that degrade cA_4 whereas the nuclease SiRe_0244 [22] is a membrane protein exhibiting very high cOA-degrading activity. Collectively, these three enzymes may work in concert to attenuate the activated CaPN enzyme in *S. islandicus*.

Downloaded from https://academic.oup.com/nar/article/53/14/gkaf744/8222437 by guest on 14 August 2025

CaPN cleaves various types of RNA *in vitro*, including cellular stable RNAs and mRNAs, and this broad-spectrum of RNase activity can yield translation arrest *in vivo*, leading to the cell enlargement and growth arrest. This is reminiscent of the results observed for over-expression of aCcr1 [68]. Currently, the mechanisms underlying the enlargement of archaeal cells remain poorly understood, and it is unclear whether this phenomenon is associated with cellular dormancy or death. Further studies are needed to investigate how CaPN functions as a cA_4-responsive effector to mediate antiviral defense and cooperates with other known cA_4-responsive effectors.

CARF-PIN fusion proteins are exclusively identified in thermophilic archaea, particularly within families such as Pyrococcaceae, Thermococcaceae, Thermofilaceae, Thermoproteaceae, Thermotogaceae, Methanocaldococcaceae, Pyrodictiaceae, Desulfurococcaceae, and Sulfolobaceae [23]. The PIN domain of CaPN exhibits RNA cleavage activity similar to that of the toxin VapC, suggesting it could be derived from fusion of two genes carrying each individual domain. Indeed, the genomic context conservation analysis on the WebFlaGs [69] site reveals that certain species carries a such pair of genes, one codes for a CARF domain while the other, a PIN domain as exemplified by Salinarchaeum sp. Harcht-Bsk1 (WP_049894480.1 and WP_020447284.1) (Supplementary Fig. S9). What occurred during evolution could several steps of adaptation: (i) the coevolution between CaPN and Type III CRISPR-Cas system, leading to the specific recognition of cOA signal by the CARF domain, (ii) the inactivation of the PIN domain in the absence of the cOA signal, and (iii) evolving of the allosteric activation of the PIN domain by CARF-cOA interaction. Strikingly, in the VapBC TA systems that are widely present in thermophiles, each VapC toxin is repressed by its cognate VapB antitoxin under the normal growth; the occurrence of certain environmental stresses inactivates the VapB, releasing VapC that cleaves varieties of cellular RNAs to inhibit cell growth [70, 71]. Here we show, upon invasion of the archaeal cells by foreign mobile genetic elements mimicked by interference plasmids, Type III CRISPR-Cas systems are activated to synthesize cOA, and the signaling molecule binds to the CARF domain of CaPN, inducing the allosteric activation of the PIN domain for RNA shredding. Noticeably, the CaPN system has the advantage of rapid activation (without the need to degrade the antitoxin) and quick recovery (the toxin can inactivate once the cOA signaling molecule degraded), compared with the VapBC systems. In this regard, CaPN can be considered as a more streamlined TA system and their sole occurrence in thermophiles may reflect both CARF and the PIN domains have more diverse functions during the thermophilic adaptation of microorganisms.

Acknowledgements

We would like to thank all the lab members of the CRISPR and Archaea Biology Research Centre for helpful discussions.

Author contributions: Yulong Shen (Writing—review & editing [supporting]).

Supplementary data

Supplementary data is available at NAR online.

Conflict of interest

None declared.

Funding

This study was supported by grants from the National Key R & D Program of China (2020YFA0906800 to Q.S.), the National Natural Science Foundation of China (Grant No. 31771380, 32270040 and 32393972), the Frontiers and Challenges Projects (SKLMTFCP-2023-05) from the State Key Laboratory of Microbial Technology at Shandong University, and project Grant No. ZR2024QC307 supported by the Shandong Provincial Natural Science Foundation. Funding to pay the Open Access publication charges for this article was provided by the National Key R & D Program of China (2020YFA0906800).

Data availability

The atomic coordinates of apo CaPN and cA_4-bound CaPN have been deposited in the Protein Data Bank under the code ID 9JXW and 9JXX, respectively.

References

1. Sorek R, Lawrence CM, Wiedenheft B. CRISPR-mediated adaptive immune systems in bacteria and archaea. *Annu Rev Biochem* 2013;**82**:237–66. https://doi.org/10.1146/annurev-biochem-072911-172315
2. Marraffini LA. CRISPR-Cas immunity in prokaryotes. *Nature* 2015;**526**:55–61. https://doi.org/10.1038/nature15386
3. Hille F, Charpentier E. CRISPR-Cas: biology, mechanisms and relevance. *Philos Trans R Soc Lond B Biol Sci* 2016;**371**:20150496. https://doi.org/10.1098/rstb.2015.0496
4. Koonin EV, Gootenberg JS, Abudayyeh OO. Discovery of diverse CRISPR-Cas systems and expansion of the genome engineering toolbox. *Biochemistry* 2023;**62**:3465–87. https://doi.org/10.1021/acs.biochem.3c00159
5. Barrangou R, Fremaux C, Deveau H *et al.* CRISPR provides acquired resistance against viruses in prokaryotes. *Science* 2007;**315**:1709–12. https://doi.org/10.1126/science.1138140
6. Makarova KS, Wolf YI, Iranzo J *et al.* Evolutionary classification of CRISPR-Cas systems: a burst of class 2 and derived variants. *Nat Rev Micro* 2020;**18**:67–83. https://doi.org/10.1038/s41579-019-0299-x
7. Altae-Tran H, Kannan S, Suberski AJ *et al.* Uncovering the functional diversity of rare CRISPR-Cas systems with deep terascale clustering. *Science* 2023;**382**:eadi1910. https://doi.org/10.1126/science.adi1910
8. Liu T, Pan S, Li Y *et al.* Type III CRISPR-Cas system: introduction and its application for genetic manipulations. *Curr Issues Mol Biol* 2018;**26**:1–14. https://doi.org/10.21775/cimb.026.001
9. Hale CR, Zhao P, Olson S *et al.* RNA-guided RNA cleavage by a CRISPR RNA-Cas protein complex. *Cell* 2009;**139**:945–56. https://doi.org/10.1016/j.cell.2009.07.040
10. Elmore JR, Sheppard NF, Ramia N *et al.* Bipartite recognition of target RNAs activates DNA cleavage by the type III-B CRISPR-Cas system. *Genes Dev* 2016;**30**:447–59. https://doi.org/10.1101/gad.272153.115
11. Kazlauskiene M, Tamulaitis G, Kostiuk G *et al.* Spatiotemporal control of type III-A CRISPR-Cas immunity: coupling DNA degradation with the target RNA recognition. *Mol Cell* 2016;**62**:295–306. https://doi.org/10.1016/j.molcel.2016.03.024
12. Yu Z, Xu J, Zhang Y *et al.* The influence of the copy number of invader on the fate of bacterial host cells in the antiviral defense by

Downloaded from https://academic.oup.com/nar/article/53/14/gkaf744/8222437 by guest on 14 August 2025

CRISPR-Cas10 DNases. *Eng Microbiol.* 2023;**3**:100102. https://doi.org/10.1016/j.engmic.2023.100102
13. Lin J, Shen Y, Ni J *et al.* A type III-A CRISPR–Cas system mediates co-transcriptional DNA cleavage at the transcriptional bubbles in close proximity to active effectors. *Nucleic Acids Res* 2021;**49**:7628–43. https://doi.org/10.1093/nar/gkab590
14. Niewoehner O, Garcia-Doval C, Rostøl JT *et al.* Type III CRISPR–Cas systems produce cyclic oligoadenylate second messengers. *Nature* 2017;**548**:543–8. https://doi.org/10.1038/nature23467
15. Kazlauskiene M, Kostiuk G, Venclovas Č *et al.* A cyclic oligonucleotide signaling pathway in type III CRISPR-Cas systems. *Science* 2017;**357**:605–9. https://doi.org/10.1126/science.aao0100
16. Han W, Stella S, Zhang Y *et al.* A type III-B cmr effector complex catalyzes the synthesis of cyclic oligoadenylate second messengers by cooperative substrate binding. *Nucleic Acids Res* 2018;**46**:10319–30.
17. Chi H, Hoikkala V, Grüschow S *et al.* Antiviral type III CRISPR signalling via conjugation of ATP and SAM. *Nature* 2023;**622**:826–33. https://doi.org/10.1038/s41586-023-06620-5
18. Jiang W, Samai P, Marraffini LA. Degradation of phage transcripts by CRISPR-associated RNases enables type III CRISPR-Cas immunity. *Cell* 2016;**164**:710–21. https://doi.org/10.1016/j.cell.2015.12.053
19. Han W, Pan S, López-Méndez B *et al.* Allosteric regulation of Csx1, a type IIIB-associated CARF domain ribonuclease by RNAs carrying a tetraadenylate tail. *Nucleic Acids Res* 2017;**45**:10740–50. https://doi.org/10.1093/nar/gkx726
20. Athukoralage JS, Rouillon C, Graham S *et al.* Ring nucleases deactivate type III CRISPR ribonucleases by degrading cyclic oligoadenylate. *Nature* 2018;**562**:277–80. https://doi.org/10.1038/s41586-018-0557-5
21. Athukoralage JS, McMahon SA, Zhang C *et al.* An anti-CRISPR viral ring nuclease subverts type III CRISPR immunity. *Nature* 2020;**577**:572–5. https://doi.org/10.1038/s41586-019-1909-5
22. Zhao R, Yang Y, Zheng F *et al.* A membrane-associated DHH-DHHA1 nuclease degrades type III CRISPR second messenger. *Cell Rep* 2020;**32**:108133. https://doi.org/10.1016/j.celrep.2020.108133
23. Makarova KS, Timinskas A, Wolf YI *et al.* Evolutionary and functional classification of the CARF domain superfamily, key sensors in prokaryotic antivirus defense. *Nucleic Acids Res* 2020;**48**:8828–47. https://doi.org/10.1093/nar/gkaa635
24. Lintner NG, Frankel KA, Tsutakawa SE *et al.* The structure of the CRISPR-associated protein Csa3 provides insight into the regulation of the CRISPR/Cas system. *J Mol Biol* 2011;**405**:939–55. https://doi.org/10.1016/j.jmb.2010.11.019
25. Baca CF, Yu Y, Rostøl JT *et al.* The CRISPR effector Cam1 mediates membrane depolarization for phage defence. *Nature* 2024;**625**:797–804. https://doi.org/10.1038/s41586-023-06902-y
26. Baca CF, Majumder P, Hickling JH *et al.* The CRISPR-associated adenosine deaminase Cad1 converts ATP to ITP to provide antiviral immunity. *Cell* 2024;**187**:7183–95.e24. https://doi.org/10.1016/j.cell.2024.10.002
27. Li Y, Li Z, Yan P *et al.* Antiviral signaling of a type III CRISPR-associated deaminase. *Science* 2025;**387**:eadr0393. https://doi.org/10.1126/science.adr0393
28. Mogila I, Tamulaitiene G, Keda K *et al.* Ribosomal stalk-captured CARF-RelE ribonuclease inhibits translation following CRISPR signaling. *Science* 2023;**382**:1036–41. https://doi.org/10.1126/science.adj2107
29. McMahon SA, Zhu W, Graham S *et al.* Structure and mechanism of a type III CRISPR defence DNA nuclease activated by cyclic oligoadenylate. *Nat Commun* 2020;**11**:500. https://doi.org/10.1038/s41467-019-14222-x
30. Zhu W, McQuarrie S, Grüschow S *et al.* The CRISPR ancillary effector Can2 is a dual-specificity nuclease potentiating type III CRISPR defence. *Nucleic Acids Res* 2021;**49**:2777–89. https://doi.org/10.1093/nar/gkab073
31. Rostøl JT, Xie W, Kuryavyi V *et al.* The Card1 nuclease provides defence during type III CRISPR immunity. *Nature* 2021;**590**:624–9.
32. Wall D, Kaiser D. Type IV pili and cell motility. *Mol Microbiol* 1999;**32**:1–10. https://doi.org/10.1046/j.1365-2958.1999.01339.x
33. Senissar M, Manav MC, Brodersen DE. Structural conservation of the PIN domain active site across all domains of life. *Protein Sci* 2017;**26**:1474–92. https://doi.org/10.1002/pro.3193
34. Schneider C, Leung E, Brown J *et al.* The N-terminal PIN domain of the exosome subunit Rrp44 harbors endonuclease activity and tethers Rrp44 to the yeast core exosome. *Nucleic Acids Res* 2009;**37**:1127–40. https://doi.org/10.1093/nar/gkn1020
35. Lamanna AC, Karbstein K. Nob1 binds the single-stranded cleavage site D at the 3′-end of 18S rRNA with its PIN domain. *Proc Natl Acad Sci USA* 2009;**106**:14259–64. https://doi.org/10.1073/pnas.0905403106
36. Anantharaman V, Aravind L. New connections in the prokaryotic toxin–antitoxin network: relationship with the eukaryotic nonsense-mediated RNA decay system. *Genome Biol* 2003;**4**:R81. https://doi.org/10.1186/gb-2003-4-12-r81
37. Bunker RD, McKenzie JL, Baker EN *et al.* Crystal structure of PAE0151 from *Pyrobaculum aerophilum*, a PIN-domain (VapC) protein from a toxin–antitoxin operon. *Proteins* 2008;**72**:510–8. https://doi.org/10.1002/prot.22048
38. Page R, Peti W. Toxin–antitoxin systems in bacterial growth arrest and persistence. *Nat Chem Biol* 2016;**12**:208–14. https://doi.org/10.1038/nchembio.2044
39. Guo L, Brügger K, Liu C *et al.* Genome analyses of Icelandic strains of *Sulfolobus islandicus*, model organisms for genetic and virus-host interaction studies. *J Bacteriol* 2011;**193**:1672–80. https://doi.org/10.1128/JB.01487-10
40. Zhai B, DuPrez K, Han X *et al.* The archaeal ATPase PINA interacts with the helicase Hjm via its carboxyl terminal KH domain remodeling and processing replication fork and Holliday junction. *Nucleic Acids Res* 2018;**46**:6627–41. https://doi.org/10.1093/nar/gky451
41. Peng N, Deng L, Mei Y *et al.* A synthetic arabinose-inducible promoter confers high levels of recombinant protein expression in hyperthermophilic archaeon *Sulfolobus islandicus*. *Appl Environ Microbiol* 2012;**78**:5630–7. https://doi.org/10.1128/AEM.00855-12
42. Deng L, Garrett RA, Shah SA *et al.* A novel interference mechanism by a type IIIB CRISPR-cmr module in *Sulfolobus*. *Mol Microbiol* 2013;**87**:1088–99. https://doi.org/10.1111/mmi.12152
43. Peng W, Feng M, Feng X *et al.* An archaeal CRISPR type III-B system exhibiting distinctive RNA targeting features and mediating dual RNA and DNA interference. *Nucleic Acids Res* 2015;**43**:406–17. https://doi.org/10.1093/nar/gku1302
44. Wei J, Li Y. CRISPR-based gene editing technology and its application in microbial engineering. *Eng Microbiol* 2023;**3**:100101. https://doi.org/10.1016/j.engmic.2023.100101
45. Peng N, Xia Q, Chen Z *et al.* An upstream activation element exerting differential transcriptional activation on an archaeal promoter. *Mol Microbiol* 2009;**74**:928–39. https://doi.org/10.1111/j.1365-2958.2009.06908.x
46. Li Y, Pan S, Zhang Y *et al.* Harnessing type I and type III CRISPR-Cas systems for genome editing. *Nucleic Acids Res* 2016;**44**:e34. https://doi.org/10.1093/nar/gkv1044
47. Deng L, Zhu H, Chen Z *et al.* Unmarked gene deletion and host-vector system for the hyperthermophilic crenarchaeon *Sulfolobus islandicus*. *Extremophiles* 2009;**13**:735–46. https://doi.org/10.1007/s00792-009-0254-2
48. Londei P, Altamura S, Cammarano P *et al.* Differential features of ribosomes and of poly(U)-programmed cell-free systems derived from sulphur-dependent archaebacterial species. *Eur J Biochem* 1986;**157**:455–62. https://doi.org/10.1111/j.1432-1033.1986.tb09689.x
49. Xiao Q, Wu T, Bao K *et al.* Upgrade of crystallography beamline BL19U1 at the shanghai synchrotron radiation facility. *J Appl*

Downloaded from https://academic.oup.com/nar/article/53/14/gkaf744/8222437 by guest on 14 August 2025

Crystallogr 2024;**57**:630–7. https://doi.org/10.1107/S1600576724002188
50. Kabsch W. XDS. *Acta Crystallogr D Biol Crystallogr* 2010;**66**:125–32. https://doi.org/10.1107/S0907444909047337
51. Minor W, Cymborowski M, Otwinowski Z *et al.* HKL-3000: the integration of data reduction and structure solution–from diffraction images to an initial model in minutes. *Acta Crystallogr D Biol Crystallogr* 2006;**62**:859–66. https://doi.org/10.1107/S0907444906019949
52. Winn MD, Ballard CC, Cowtan KD *et al.* Overview of the CCP4 suite and current developments. *Acta Crystallogr D Biol Crystallogr* 2011;**67**:235–42. https://doi.org/10.1107/S0907444910045749
53. Emsley P, Lohkamp B, Scott WG *et al.* Features and development of Coot. *Acta Crystallogr D Biol Crystallogr* 2010;**66**:486–501. https://doi.org/10.1107/S0907444910007493
54. Liebschner D, Afonine PV, Baker ML *et al.* Macromolecular structure determination using X-rays, neutrons and electrons: recent developments in Phenix. *Acta Crystallogr D Struct Biol* 2019;**75**:861–77. https://doi.org/10.1107/S2059798319011471
55. Krissinel E, Henrick K. Inference of macromolecular assemblies from crystalline state. *J Mol Biol* 2007;**372**:774–97. https://doi.org/10.1016/j.jmb.2007.05.022
56. Sofos N, Feng M, Stella S *et al.* Structures of the cmr-β complex reveal the regulation of the immunity mechanism of type III-B CRISPR-Cas. *Mol Cell* 2020;**79**:741–57. https://doi.org/10.1016/j.molcel.2020.07.008
57. Yu Z, Jiang S, Wang Y *et al.* CRISPR-Cas adaptive immune systems in Sulfolobales: genetic studies and molecular mechanisms. *Sci China Life Sci* 2021;**64**:678–96. https://doi.org/10.1007/s11427-020-1745-0
58. Matelska D, Steczkiewicz K, Ginalski K. Comprehensive classification of the PIN domain-like superfamily. *Nucleic Acids Res* 2017;**45**:6995–7020. https://doi.org/10.1093/nar/gkx494
59. Garcia-Doval C, Schwede F, Berk C *et al.* Activation and self-inactivation mechanisms of the cyclic oligoadenylate-dependent CRISPR ribonuclease Csm6. *Nat Commun* 2020;**11**:1596. https://doi.org/10.1038/s41467-020-15334-5
60. Molina R, Jensen ALG, Marchena-Hurtado J *et al.* Structural basis of cyclic oligoadenylate degradation by ancillary type III CRISPR-Cas ring nucleases. *Nucleic Acids Res* 2021;**49**:12577–90. https://doi.org/10.1093/nar/gkab1130
61. Holm L. Dali server: structural unification of protein families. *Nucleic Acids Res* 2022;**50**:W210–5. https://doi.org/10.1093/nar/gkac387
62. Molina R, Stella S, Feng M *et al.* Structure of Csx1-cOA(4) complex reveals the basis of RNA decay in type III-B CRISPR-Cas. *Nat Commun* 2019;**10**:4302. https://doi.org/10.1038/s41467-019-12244-z
63. Jia N, Jones R, Yang G *et al.* CRISPR-Cas III-A Csm6 CARF domain is a ring nuclease triggering stepwise cA4 cleavage with ApA>p formation terminating RNase activity. *Mol Cell* 2019;**75**:944–56.
64. Zhang D, Du L, Gao H *et al.* Structural insight into the Csx1–Crn2 fusion self-limiting ribonuclease of type III CRISPR system. *Nucleic Acids Res* 2024;**52**:8419–30. https://doi.org/10.1093/nar/gkae569
65. Jungfer K, Sigg A, Jinek M. Substrate selectivity and catalytic activation of the type III CRISPR ancillary nuclease Can2. *Nucleic Acids Res* 2024;**52**:462–73. https://doi.org/10.1093/nar/gkad1102
66. Lowey B, Whiteley AT, Keszei AFA *et al.* CBASS immunity uses CARF-related effectors to sense 3′-5′- and 2′-5′-linked cyclic oligonucleotide signals and protect bacteria from phage infection. *Cell* 2020;**182**:38–49. https://doi.org/10.1016/j.cell.2020.05.019
67. Molina R, Garcia-Martin R, Lopez-Mendez B *et al.* Molecular basis of cyclic tetra-oligoadenylate processing by small standalone CRISPR-Cas ring nucleases. *Nucleic Acids Res* 2022;**50**:11199–213. https://doi.org/10.1093/nar/gkac923
68. Yang Y, Liu J, Fu X *et al.* A novel RHH family transcription factor aCcr1 and its viral homologs dictate cell cycle progression in archaea. *Nucleic Acids Res* 2023;**51**:1707–23. https://doi.org/10.1093/nar/gkad006
69. Saha CK, Sanches Pires R, Brolin H *et al.* FlaGs and webFlaGs: discovering novel biology through the analysis of gene neighbourhood conservation. *Bioinformatics* 2021;**37**:1312–4. https://doi.org/10.1093/bioinformatics/btaa788
70. Thakur Z, Chaudhary R, Mehta PK. Deciphering the role of VapBC toxin–antitoxin systems in *Mycobacterium tuberculosis* stress adaptation. *Future Microbiol* 2024;**19**:1587–99. https://doi.org/10.1080/17460913.2024.2412447
71. Lin J, Guo Y, Yao J *et al.* Applications of toxin–antitoxin systems in synthetic biology. *Eng Microbiol* 2023;**3**:100069. https://doi.org/10.1016/j.engmic.2023.100069

Downloaded from https://academic.oup.com/nar/article/53/14/gkaf744/8222437 by guest on 14 August 2025

Received: April 30, 2025. **Revised:** July 2, 2025. **Editorial Decision:** July 6, 2025. **Accepted:** July 17, 2025
© The Author(s) 2025. Published by Oxford University Press.
This is an Open Access article distributed under the terms of the Creative Commons Attribution-NonCommercial License (https://creativecommons.org/licenses/by-nc/4.0/), which permits non-commercial re-use, distribution, and reproduction in any medium, provided the original work is properly cited. For commercial re-use, please contact reprints@oup.com for reprints and translation rights for reprints. All other permissions can be obtained through our RightsLink service via the Permissions link on the article page on our site—for further information please contact journals.permissions@oup.com.